Thermal diffusivity measurement of single fibers by an ac calorimetric method

Tsuneyuki Yamane, Shinichiro Katayama, Minoru Todoki, and Ichiro Hatta

Citation: Journal of Applied Physics **80**, 4358 (1996); doi: 10.1063/1.363394
View online: http://dx.doi.org/10.1063/1.363394
View Table of Contents: http://scitation.aip.org/content/aip/journal/jap/80/8?ver=pdfcov
Published by the AIP Publishing

Thermal diffusivity measurement of single fibers by an ac calorimetric method

Tsuneyuki Yamane, Shin-ichiro Katayama, and Minoru Todoki
Materials Characterization Laboratories, Toray Research Center, Inc., Otsu, Shiga 520, Japan

Ichiro Hatta
Department of Applied Physics, School of Engineering, Nagoya University, Chikusa-ku, Nagoya 464-01, Japan

(Received 25 April 1996; accepted for publication 8 July 1996)

An ac calorimetric method is applied to the direct measurement of thermal diffusivity of single fibers. Theoretical analysis is presented, taking into account the two-dimensional ac thermal wave for cylindrical systems and the effect of time delay at the temperature detecting system. Experimental tests are performed using nickel and stainless steel wires about 20 μm in diameter. The thermal conductivity of fibers about 10 μm in diameter of the advanced materials, polyacrylonitrile-based carbon, TORAYCA, and aramide, Kevlar, is determined. The relationship between the thermal conductivity and electric conductivity and the crystalline size of these fibers is discussed. For composite materials made of carbon fibers, the observed thermal conductivity agrees with the thermal conductivity estimated using the values determined by the present method. © *1996 American Institute of Physics.* [S0021-8979(96)00720-7]

I. INTRODUCTION

The development of new types of fibers for use as mechanical reinforcing agents in various composites is progressing. Measurement of the thermal conductivity of these fibers is important, as is that of mechanical properties, to design practical devices using these fibers. On the other hand, from the fundamental point of view, measurement of temperature dependence of thermal diffusivity allows investigation of the microstructure of the fibers, i.e., structural defects and phonon–phonon interactions.[1] Some methods based on the steady state method have been developed to measure the thermal conductivity of these single-filament fibers directly.[2,3] Since these fibers usually have very small diameter, about 0.01 mm, and heat loss from the sample is large, these methods require a complicated technique to reduce the heat loss from the sample. Thermal conductivity can also be derived from the relation

$$\lambda = \rho C_p D, \tag{1}$$

where ρ is the density, C_p is the specific heat capacity, and D is the thermal diffusivity. Thermal diffusivity can be obtained using a variety of nonsteady state methods. Recently, the photothermal beam deflection method was applied to the direct measurement of thermal diffusivity for thin single-filament wires,[4] this method requires a special technique involving the use of two laser beams as the heat source and the temperature detector. A light-irradiation ac calorimetric method is superior for the measurement of thermal diffusivity of thin film,[5] and has also been applied to thin wires.[6] In the studies reported, thermal diffusivity is obtained from the decay constant of the ac temperature wave amplitude, as a function of the distance between the edge of the shading mask and a temperature sensor attached to the sample lying under the mask, assuming that the propagation of the ac temperature wave is one dimensional. Assuming there is no heat loss from the sample, the decay constant, k, is given by

$$k = \sqrt{\frac{\pi f}{D}}, \tag{2}$$

where f is the ac frequency of the irradiated light. The sample dimensions required for precise measurement in a platelike sample have been theoretically and experimentally discussed in detail.[7–9] This method does not require a complicated measurement system, and can be used to estimate the degree of heat loss from the sample based on the ac frequency dependence of the observed thermal diffusivity. In this article, first we theoretically consider the criterion for the sample dimensions when we apply this method to a thin wire, i.e., a cylindrical system, and the effect of the time delay at the temperature detecting system. Next, we experimentally check the applicability of this method to a thin metal wire, the thermal diffusivity of which is well known. Finally, we apply this method to typical advanced fibers used as mechanical reinforcing agents in various composites, i.e., polyacrylonitrite-based carbon fibers and aramide fibers.

II. THEORY

We consider a cylindrical sample composed of an infinite rod with radius a as shown in Fig. 1. The heat conduction equation for an isotropic medium with thermal diffusivity, D, is

$$\frac{\partial^2 T(x,r,t)}{\partial r^2} + \frac{1}{r}\frac{\partial T(x,r,t)}{\partial r} + \frac{\partial^2 T(x,r,t)}{\partial x^2} + \frac{Q(x,r,t)}{Dc} - \frac{1}{D}\frac{\partial T(x,r,t)}{\partial t} = 0, \tag{3}$$

where c is the heat capacity per unit volume. If there is any heat flow over the surface, the boundary condition at $r=a$ is

$$\frac{\partial T(x,r,t)}{\partial r} - \frac{L}{a}T(x,r,t) = 0 \quad \text{for } r=a, \tag{4}$$

 0021-8979/96/80(8)/4358/8/$10.00

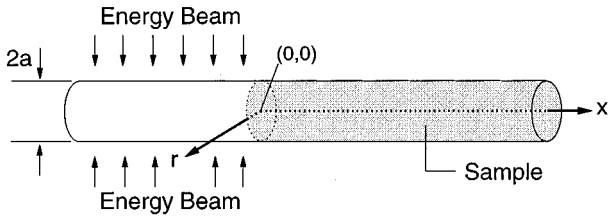

FIG. 1. A schematic view of a thermal diffusivity measurement system for a single fiber. The sample is an infinite rod. The ac thermal energy is supplied to the sample surface in the region $x<0$.

where L is the Biot number defined as

$$L=\frac{a\delta}{cD}, \tag{5}$$

where δ is the thermal conductance per unit area. When an ac thermal energy

$$Q(x,r,t)=Q_0\ \exp(i2\pi ft) \quad \text{for } x<0 \text{ and } r=a \tag{6}$$

is supplied over the sample, the ac temperature response, $T(x,r,f)$, is numerically obtained from the Fourier transform of $T(x,r,t)$, which is the temperature response for the impulse thermal energy[9]

$$Q(x,r,t)=Q_0\delta(t) \quad \text{for } x<0 \text{ and } r=a. \tag{7}$$

$T(x,r,t)$ is represented as

$$T(x,r,t)=T_0T_x(x,t)T_r(r,t), \tag{8}$$

where $T_0=2Q_0/ca$, $T_x(x,t)$ is the x component, and $T_r(r,t)$ is the r component.[10] For the x component, $T_x(x,t)$, the temperature at time t, is given by[10]

$$T_x(x,t)=\frac{1+\mathrm{erf}\left(-\frac{x}{2x_c}\sqrt{\frac{t_c}{t}}\right)}{2} \quad \text{for } x<0, \tag{9}$$

$$T_x(x,t)=\frac{1-\mathrm{erf}\left(\frac{x}{2x_c}\sqrt{\frac{t_c}{t}}\right)}{2} \quad \text{for } x\geqslant 0, \tag{10}$$

where t_c is the characteristic time defined by

$$t_c=\frac{a^2}{D}, \tag{11}$$

x_c is the characteristic length defined by

$$x_c=\frac{a}{\pi}, \tag{12}$$

and $\mathrm{erf}(x)$ is the error function. For the r component, $T_r(r,t)$, the temperature at time t is given by[10]

$$T_r(r,t)=\sum_{n=1}^{\infty}\frac{Z_i^2J_0(Z_ir/a)J_0(Z_i)}{(Z_i^2+L^2)J_0^2(Z_i)}\exp\left(-Z_i^2\frac{t}{t_c}\right), \tag{13}$$

where J_0 is the Bessel function of the first kind of order 0 and Z_i $(i=1,2,3,...,)$ are positive roots of

$$Z_iJ_1(Z_i)-LJ_0(Z_i)=0, \tag{14}$$

where J_1 is the Bessel function of the first kind of order 1.

If there is no temperature gradient in the direction of the r axis, we can regard the system as a one-dimensional thermal system. The solution of Eq. (3) is analytically obtained as[11]

$$\overline{T}(x,r,f)=\frac{Q_0\ \exp(i2\pi ft)}{i\omega ca+\delta}\times\left(-\sqrt{\frac{i\omega ca+\delta}{caD}}\,x\right) \quad \text{for } x>0 \text{ and } 0<r<a. \tag{15}$$

From Eq. (15), $|\overline{T}(x,r,f)|$ is obtained from

$$|\overline{T}(x,r,f)|=\frac{Q_0}{\pi fca\sqrt{1+(1/\omega\tau_e)^2}}\times\exp(-kx) \quad \text{for } x>0 \text{ and } 0<r<a, \tag{16}$$

where k is the decay constant defined as

$$k=\sqrt{\frac{\pi f}{D^*}}=\sqrt{\frac{\pi f}{D}}\left(\sqrt{\frac{\sqrt{1+(1/2\pi f\tau_e)^2}+1}{2}}+\sqrt{\frac{\sqrt{1+(1/2\pi f\tau_e)^2}-1}{2}}\right), \tag{17}$$

where τ_e is an external relaxation time defined as

$$\tau_e=\frac{ca}{\delta}, \tag{18}$$

that is,

$$\tau_e=\frac{t_c}{L}. \tag{19}$$

From the measurement of the x dependence of $\ln|\overline{T}(x,r,f)|$, we obtain the value of the decay constant, k, from which the apparent thermal diffusivity, D^* along the x direction can be estimated using Eq. (17). The real thermal diffusivity, D, can be determined from the frequency dependence of the apparent thermal diffusivity, D^* with

$$\frac{1}{D^*}=\frac{1}{D}\left[\sqrt{1+\left(\frac{1}{2\pi f\tau_e}\right)^2}+\frac{1}{2\pi f\tau_e}\right]. \tag{20}$$

For platelike samples, we have confirmed that, apart from the region $x>100d/\pi$, the system can be considered as a one-dimensional system, where d is the sample thickness.[9] We estimate the criterion used to approximate the cylindrical system to a one-dimensional system in the same manner using the above equations. Figure 2 shows the ac temperature amplitude at the sample surface, $\ln|\overline{T}(x,a,f)|/\sqrt{f/f_c}$, which is derived from the Fourier transform of Eq. (8), versus the nondimensional distance, x/x_c, for $L=0.000\,001$ and $f/f_c=0.000\,0005$–$0.000\,01$, where f_c is the characteristic frequency defined by

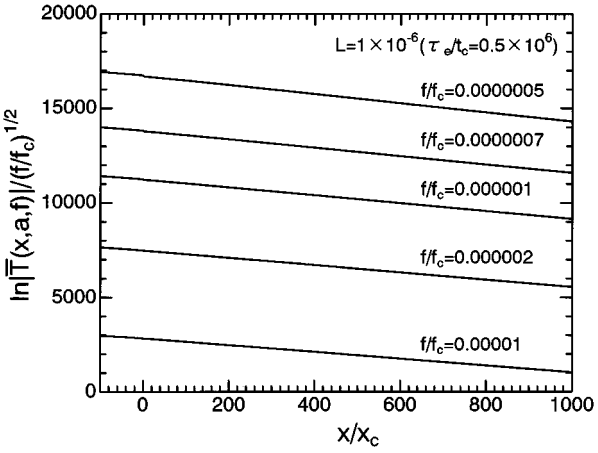

FIG. 2. The ac temperature amplitude, which is derived from the Fourier transform of Eq. (8), vs nondimensional distance for $L=0.000\,001$ and $f/f_c=0.000\,0005$–$0.000\,01$.

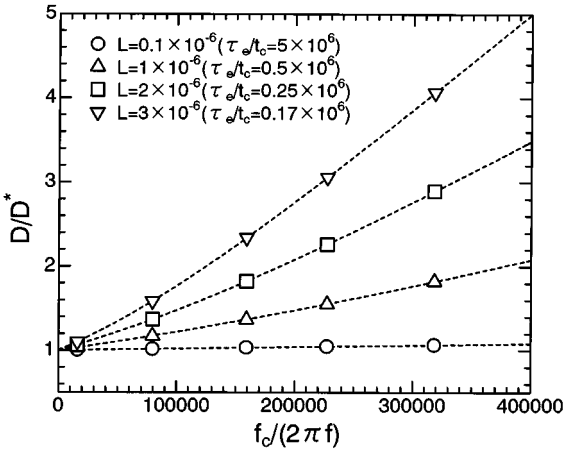

FIG. 4. The dependence of the inverse of the normalized apparent thermal diffusivity on the inverse of the nondimensional frequency obtained from the amplitude of ac temperature for $L=0.000\,0001$–$0.000\,003$. The dashed lines are values calculated using the analytical one-dimensional solution of Eq. (20).

$$f_c=\frac{D}{a^2}. \tag{21}$$

For $x/x_c>0$, $\ln|\overline{T(x,a,f)}|/\sqrt{f/f_c}$ decays with a constant slope. Figure 3 shows the relation $D^*(x)/D$ vs x/x_c for $L=0.000\,001$ and $f/f_c=0.000\,0005$–$0.000\,01$ derived from the curve in Fig. 2. $D^*(x)/D$ is estimated as

$$\frac{D^*(x)}{D}=\frac{\pi}{k(x)^2}, \tag{22}$$

where $k(x)$ is the decay constant, which is determined by the partial derivative of $\ln|\overline{T(x,a,f)}|/\sqrt{f/f_c}$ with respect to x/x_c for each point,

$$k(x)=\frac{\partial[\ln|\overline{T(x,a,f)}|/\sqrt{f/f_c}]}{\partial(x/x_c)}. \tag{23}$$

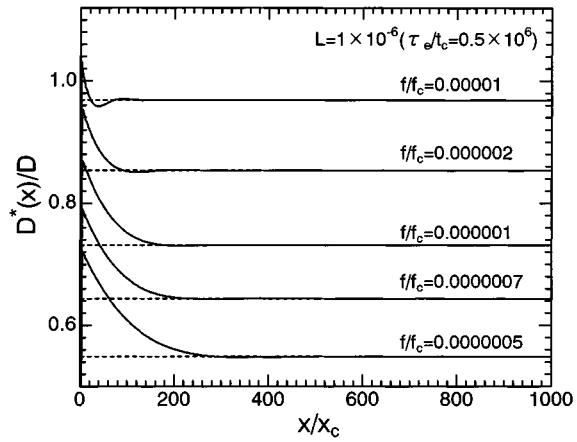

FIG. 3. Normalized apparent thermal diffusivity estimated using Eq. (22) vs nondimensional distance for $L=0.000\,001$ and $f/f_c=0.000\,0005$–$0.000\,01$. The decay constant $k(x)$ is determined using Eq. (23) for each point. The dashed lines are values calculated using the analytical one-dimensional solution of Eq. (20).

The dashed lines are values calculated using the analytical one-dimensional solution of Eq. (20). Figure 3 shows that, apart from in the region $x/x_c>500$, the slope of $\ln|\overline{T(x,a,f)}|/\sqrt{f/f_c}$, namely, the observed thermal diffusivity is constant and agrees with the values of the one-dimensional solution. Figure 4 shows the dependence of the inverse of the normalized apparent thermal diffusivity, D/D^*, on the inverse of the nondimensional frequency, f_c/f, for $L=0.0002$–$0.000\,01$, where the normalized apparent thermal diffusivity is estimated from the constant slope of the amplitude of ac temperature in the region $x/x_c>500$ as shown in Fig. 3. The dashed lines are values calculated using the analytical one-dimensional solution of Eq. (20). From Figs. 2–4, the cylindrical system can be considered as a one-dimensional system in the region $x/x_c>500$, i.e., $x>500a/\pi$, which is similar to the case of platelike samples.

In the present measurement, the ac light impinges only on the semicircular surface of the fiber. We consider the effect of a cylindrically nonuniform supplied energy for the ac temperature response. When a cylindrically nonuniform ac thermal energy

$$Q(x,r,\theta,t)=Q_0Q(\theta)\exp(i2\pi ft) \quad \text{for } x<0 \text{ and } r=a, \tag{24}$$

where $Q(\theta)$, the cylindrical distribution of energy, is supplied over the sample, the ac temperature response, $T(x,r,\theta,f)$, is numerically obtained from the Fourier transform of $T(x,r,\theta,t)$, which is the temperature response for the impulse thermal energy

$$Q(x,r,\theta,t)=Q_0Q(\theta)\delta(t) \quad \text{for } x<0 \text{ and } r=a. \tag{25}$$

$T(x,r,\theta,t)$ is represented as

$$T(x,r,\theta,t)=T_0T_x(x,t)T_r(r,t)T_\theta(\theta,t), \tag{26}$$

where $T_\theta(\theta,t)$ is the cylindrical component. The theoretical results for cylindrically uniform supplied energy represented by Figs. 2–4 were obtained from the Fourier transform of

TABLE I. Physical properties of carbon fibers and aramide fibers at 298.15 K.

Sample	Tensile strength (GPa)	Young's modulus (GPa)	Density ρ (10^3 kg m^{-3})	Specific heat capacity C_p (kJ kg^{-1} K^{-1})	Electric conductivity σ (10^4 Ω^{-1} m^{-1})	Crystalline size L_c (10^{-7} m)	Crystalline size L_{004} (10^{-9} m)
Torayca							
T300	3.53	230	1.76	0.759	5.91	1.7[a]	···
T300J	4.41	230	1.82	0.758	6.56	···	···
T800H	5.59	294	1.81	0.754	7.18	1.9[a]	···
M35J	5.00	343	1.75	0.724	8.97	···	···
M40J	4.40	377	1.77	0.720	9.77	3.3[a]	···
M46J	4.20	436	1.84	0.721	10.7	4.1[a]	···
M50J	4.02	475	1.87	0.716	11.3	4.9[a]	···
M60J	3.82	588	1.94	0.721	12.7	6.2[a]	···
M30	3.92	294	1.70	0.732	8.32	2.2[a]	···
M46	2.55	451	1.88	0.719	12.1	5.1[a]	···
M50	2.45	490	1.91	0.718	13.1	5.9[a]	···
Kevlar							
29	2.90	71.8	1.44	1.28	···	···	20[b]
49	2.80	109	1.45	1.25	···	···	21[b]
149	2.30	144	1.47	1.13	···	···	27[b]

[a]See Ref. 14.
[b]See Ref. 15.

$T(x,r,t)$ in Eq. (8). Far from the boundary between the heated and nonheated regions, i.e., $x>500a/\pi$, the time dependence of $T(x,r,t,)$ is as follows. In the short time region, $T(x,r,t)$ is approximately zero, because the x component, $T_x(x,t)$, is approximately zero although the r component, $T_x(x,t)$, is changing. In the long time region, the time dependence of $T(x,r,t)$ becomes the same as $T_x(x,t)$, because $T_r(r,t)$ becomes constant. These time dependences derive the one-dimensional ac temperature wave propagation over the regions of $x>500a/\pi$ shown in Figs. 2–4. In Eq. (26), the component $T_r(r,t)T_\theta(\theta,t)$ becomes constant in the long time region far from the boundary between the heated and nonheated regions, which is the same as $T_r(r,t)$ in Eq. (8). This means that far from the boundary between the heated and nonheated regions the results for cylindrically uniform supplied energy shown in Figs. 2–4 should be held under the conditions of Eq. (24). It is concluded from this consideration that there should be a region where the slope of the curve of $\ln|T(x,a,f)|$ vs x is constant, and the ac temperature wave propagation can be considered as a one-dimensional system that is independent of the cylindrical distribution of the supplied energy, $Q(\theta)$.

In previous work[5,6] and in this study, a thermocouple is used as the temperature detector because of its high sensitivity and ease of use. The contribution of an adhesive that attaches the thermocouple to the sample is discussed.[12] Another non-negligible effect when a thermocouple is used as the temperature detector is the time delay in measuring the temperature. Based on system design that takes into account the time delay affect, when the impulse thermal energy, represented by Eq. (7), is supplied to the sample, the temperature response detected by the temperature detecting system at the position $r=a$ with respect to time t, $T_{\rm obs}(x,a,t)$, is expressed in the following convolution equation:

$$T_{\rm obs}(x,a,t)=\int_{x-b/2}^{x-b/2}\int_0^t T(x',a,\eta)g(t-\eta)\,d\eta\,dx', \quad (27)$$

where b is the area of contact, $g(t)$ is the impulse response of the temperature detecting the system, and η is a parameter, assuming the temperature detecting system responds linearly to the real temperature. Taking the Fourier transform of Eq. (27) with respect to t, we obtain

$$|\overline{T}_{\rm obs}(x,a,f)|=\int_{x-b/2}^{x-b/2}|\overline{T}(x',a,f\ )\|G(f\ )|dx', \quad (28)$$

where $|G(f\ )|$ is the transfer function of thermocouple. From the above consideration, ac temperature amplitude, $|T(x,a,f\ )|$, can be expressed by Eq. (16) in the region $x>500a/\pi$. Using this relation, Eq. (28) can be expressed as

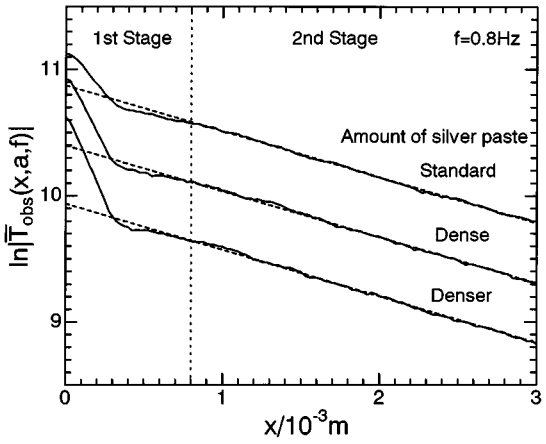

FIG. 5. Typical plot of $\ln|\overline{T}_{\rm obs}(x,a,f\ )|$ vs distance x for thin nickel wire 25 μm in diameter at 298.15 K. The chopping frequency is 0.8 Hz. The solid line indicates experimental data. Two stages can be seen, denoted by 1st and 2nd stages. For the upper curve the amount of silver paste is the same as in the standard experiment. For the middle and bottom curves, silver paste was added after the measurement for the standard experiment was performed. The dashed lines represent results calculated using linear equations, the coefficients of which are shown in Table II.

TABLE II. Apparent thermal diffusivities of nickel wire measured by the ac calorimetric method at 298.15 K. Slope and intercept are the values for the dashed line in Fig. 5. The apparent thermal diffusivity is determined from Eq. (31) using the slope indicated below.

Amount of silver paste	Slope k (10^2 m^{-1})	Intercept	Apparent thermal diffusivity D^* (10^{-4} m^2 s^{-1})
Standard	−3.63	10.9	0.191
Dense	−3.63	10.4	0.191
Denser	−3.68	9.94	0.186

$$|\overline{T_{\rm obs}}(x,a,f)| = \int_{x-b/2}^{x-b/2} A\ \exp(-kx')|G(f\ )|dx', \qquad (29)$$

where A is constant. Accordingly

$$|\overline{T_{\rm obs}}(x,a,f)| = A\ \frac{\exp(b/2)+\exp(-b/2)}{k} \times \exp(-kx)|G(f)|. \qquad (30)$$

In Eq. (30), $|G(f)|$ can be considered to be independent of x. Therefore

$$\ln|\overline{T_{\rm obs}}(x,a,f)| = \text{const} - kx \quad \text{for } x > 500a/\pi \text{ and } 0 < r < a. \qquad (31)$$

Equation (31) shows that the observed decay constant of ac temperature wave amplitude in the x direction is constant if there is any time delay in the temperature detecting system.

III. EXPERIMENT

The experiment was performed using a commercially available apparatus (Sinku-Riko Inc., type PIT-1). The construction of the apparatus is detailed in Ref. 5. An oscillatory heat flux with frequency f was supplied on the semicircular surface of the fiber by means of chopped light from a tungsten halogen lamp. The resulting ac temperature wave amplitude $|\overline{T_{\rm obs}}(x,a,f\ )|$ was detected using a Chromel–Alumel thermocouple wire (12.5 μm in diameter) that was attached with silver paste to the middle of the fiber. The sample was a single filament about 50 mm long. The distance x between the thermocouple and the edge of the shading mask was changed by moving the mask. The measurements were performed in vacuum ($<10^{-5}$ Torr) to reduce the heat loss from the fibers.

Nickel (25 μm in diameter) and stainless steel (20 μm in diameter) are used as the test samples the bulk thermal diffusivities of which have been reported.[13] For application to industrial materials, polyacrylonitrite (PAN)-based carbon fiber (CF) Torayca, supplied by Toray Industries, Inc., and aramide [poly-(p-phenylene terephthalamide)] fiber (AF) Kevlar, supplied by Du Pont Toray Kevlar, Ltd., are measured. The diameter of the CFs is about 7 μm and that of the AFs is about 12 μm. Table I shows the physical properties of these CFs and AFs. In Table I, the M series is a high-modulus type, the MJ series is a high-modulus and high-strength type, and the T series is a high-tenacity type of CFs. The crystal size was determined by x-ray diffraction measurement. For CFs, crystalline size is calculated from the intensity profile of (002) reflections.[14] For AFs, it is calculated from the intensity profile of (004) reflections.[15] For CFs, the crystalline size, L_c, is the thickness of the stacked graphite-layer planes parallel to the fiber axis. For AFs, the crystalline size, L_{004} is the thickness of the (004) planes normal to the fiber axis. Specific heat capacity, C_p, was measured by a heat-compensation-type differential scanning calorimeter (DSC) (Perkin-Elmer Corp., type DSC-2), using sapphire as the standard material. The surface of AFs were coated with bismuth film to absorb irradiated light effectively, as done in the case of the polymer films.[16] The thickness of the deposited bismuth film is about 0.05 μm which is estimated from the weight of bismuth vaporized. It is experimentally confirmed that a bismuth layer in this thickness range does not affect the thermal diffusivity because the grains in the deposited film are small.[16]

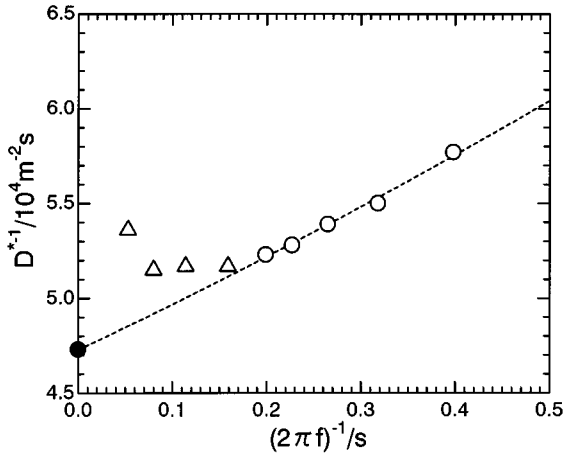

FIG. 6. Frequency dependence of the apparent thermal diffusivity D^* for thin nickel wire 25 μm in diameter at 298.15 K. The open circles and triangles represent experimental data. The dashed line represents the values calculated using Eq. (20). The closed circles agree with the real thermal diffusivity D.

TABLE III. Thermal diffusivities in thin wires measured by the ac calorimetric method at 298.15 K, together with those from TPRC (after Ref. 13).

Sample	Diameter a (10^{-6} m)	Frequency range f (Hz)	Thermal diffusivity D (10^{-4} m^2 s^{-1})	Relaxation time τ_e(s)	Thermal diffusivity from the TPRC[a] D (10^{-4} m^2 s^{-1})
Nickel	20	0.4–0.8	0.212	2.02	0.15–0.25
Stainless steel	20	0.03–0.1	0.0373	4.83	0.032–0.037

[a]Reference 13.

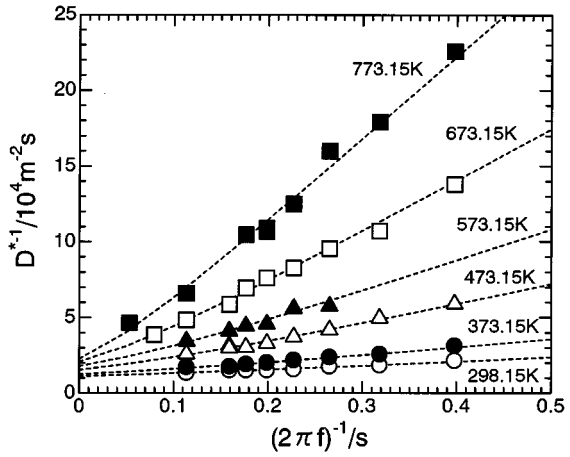

FIG. 7. Frequency dependence of the apparent thermal diffusivity D^* at various temperatures for the CF single filament (Torayca, type M50) about 7 μm in diameter. The dashed line represents the calculated values.

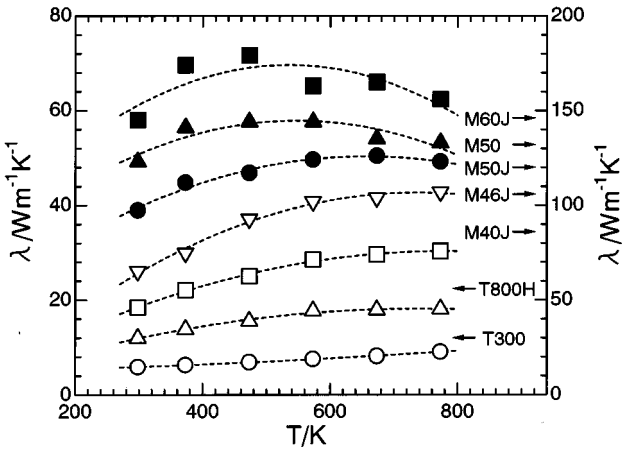

FIG. 8. Temperature dependence of the thermal conductivity of CFs in the temperature range of 298.15–773.15 K.

IV. RESULTS

A. Metallic wire

Figure 5 shows a typical plot of $\ln|\overline{T_{\rm obs}}(x,a,f)|$ at 298.15 K. $|T_{\rm obs}(x,a,f)|$ is the voltage from the thermocouple that is proportional to the ac temperature response. In Fig. 5, the difference in the three curves is due to the difference in the amount of silver paste used to attach the thermocouple to the sample. For the upper curve the amount of silver paste is the same as in the standard experiment. For the middle and bottom curves, silver paste was added after the measurement for the standard experiment was performed. Two stages are observed in all the curves of $\ln|T_{\rm obs}(x,a,f)|$ vs x as discussed in Ref. 5 for measurement of stainless steel using a spot-welded thermocouple as the temperature detector. In the first stage, $\ln|T_{\rm obs}(x,a,f)|$ decays rapidly. This may be due to the fact that the heat capacity of the silver paste is larger than that of the fiber. In the second stage, $\ln|T_{\rm obs}(x,a,f)|$ decays according to Eq. (31). The data in this stage were analyzed to determine the apparent thermal diffusivity, D^*, by a least-squares fit to Eq. (31). The calculated curve is shown in Fig. 5 by the dashed line, of which the slope and intercept are given in Table II. Figure 5 and the results in Table II show that, as the amount of silver paste becomes large, and although $\ln|T_{\rm obs}(x,a,f)|$ becomes small and noisy, the decay constant of x dependence of $\ln|T_{\rm obs}(x,a,f)|$ remains constant. From the above theoretical consideration summarized in Eq. (31), the decay constant of x dependence of $\ln|T_{\rm obs}(x,a,f)|$ is independent of the transfer function of the temperature detecting system, i.e., of the thermocouple and adhesive. Figure 5 and the results in Table II actually demonstrate the validity of the theoretical consideration.

Figure 6 shows the relationship between the inverse of apparent thermal diffusivity, D^*, and the inverse of the ac angular frequency $2\pi f$ for nickel wire at 298.15 K. The data, which are denoted by open circles, were analyzed by a least-squares fit to Eq. (20). The curve in Fig. 6 shown with a dashed line is calculated using $D=0.211\times10^{-4}$ m^2 s^{-1} and $\tau_e=2.02$ s. Accordingly $\tau_e/t_c=0.273\times10^6$, i.e., $L=1.83\times10^{-6}$. Therefore, when $2\pi f=\infty$, D^* becomes the real thermal diffusivity D in Fig. 6 that is denoted by the closed circles. At high frequencies, the observed apparent thermal diffusivity, which is shown by the open triangles, deviates from the dashed line. This is because the ac temperature detecting system does not respond linearly to the real ac temperature change.

Table III shows a comparison between the results obtained by the present ac calorimetric method and TPRC recommended values.[13] The present results agree with those for bulk materials. There is no significant difference between the values in the thin wire and the bulk.

B. Advanced materials

Figure 7 shows the relationship between the inverse of the apparent thermal diffusivity D^* and the inverse of the ac angular frequency $2\pi f$ for CF of type M50 at various temperatures. As the temperature increases, the slope of the

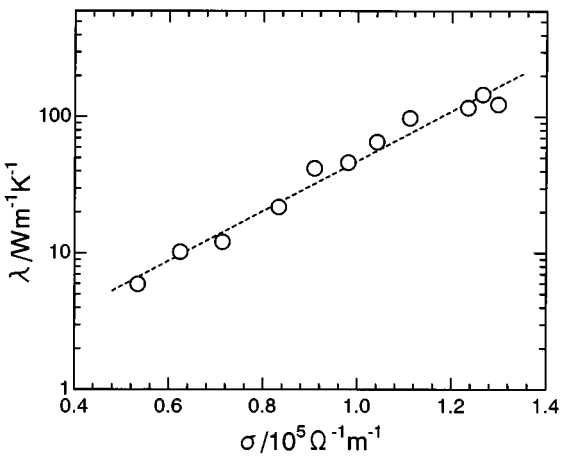

FIG. 9. The thermal conductivity vs electric conductivity of CFs at 298.15 K. If the Wiedemann–Franz law holds as in pure metals, thermal conductivity of CFs is in the range of 0.43–0.96 W m^{-1} K^{-1}.

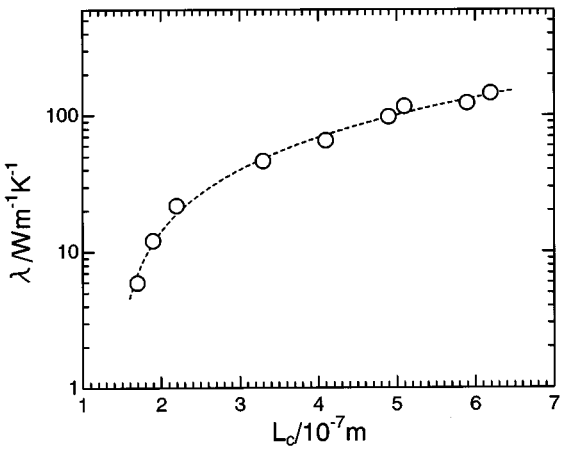

FIG. 10. Dependence of the thermal conductivity of CFs on the crystalline size at 298.15 K. The crystalline size, L_c, is the thickness of the stacked graphite-layer plane parallel to the fiber axis.

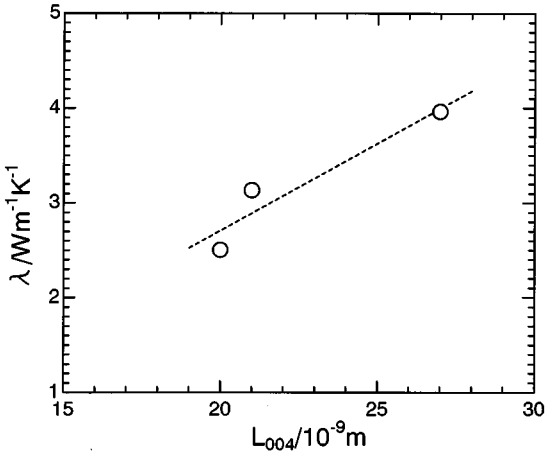

FIG. 11. Dependence of the thermal conductivity of AFs on the crystalline size at 298.15 K. The crystalline size, L_{004} is the thickness of the (004) planes normal to the fiber axis.

dashed line increases because the external relaxation time becomes short, e.g., $\tau_e=0.606$ s at 298.15 K, $\tau_e=0.224$ s at 473.15 K, and $\tau_e=0.0820$ s at 773.15 K.

Figure 8 shows the temperature dependence of the thermal conductivity of the CFs above 298.15 K. The density at 298.15 K in Table I is adopted as the density up to 298.15 K to calculate the thermal conductivity using Eq. (2). The thermal conductivitise of T300, T800H, M40J, M46J, and M50J increase linearly as the temperature increases. The thermal conductivities of M50 and M60J increase below 500 K and decrease above 500 K, as temperature increases. This behavior may reflect the growth of graphite crystals in the CFs.

From the fundamental point of view, we compare the thermal conductivity determined using the ac calorimetric method with the other properties in Table I. Figure 9 shows the thermal conductivity versus electric conductivity at 298.15 K. If the Wiedemann–Franz law holds as in pure metals, the electronic contribution to the thermal conductivity of CF can be estimated, e.g., 0.43 $\mathrm{W\,m^{-1}\,K^{-1}}$ for T300, and 0.96 $\mathrm{W\,m^{-1}\,K^{-1}}$ for M50. These are far smaller than the presently obtained values, 5.90 and 123 $\mathrm{W\,m^{-1}\,K^{-1}}$ at 298.15 K, respectively. This indicates the well-known fact that thermal conduction may be mainly due to phonons for PAN-based CFs. This result agrees with the result for graphite.[17] Figures 10 and 11 show the dependence of thermal conductivity on crystalline size. The thermal conductivity of CFs and AFs increases as the crystalline size increases. This result shows that the degree of ordering of crystalline regions in the sample governs the thermal conduction for these materials, which agrees with the results generally obtained for insulators.[1]

From the practical point of view, we apply the results for CFs to a unidirectional carbon fiber reinforced plastic (CFRP) composite that is prepared by the following procedure. CFs were impregnated with a toughened epoxy resin and a unidirectional prepreg sheet was formed by drum winding, followed by hot pressing. The prepreg was cured in an autoclave at 450 K for 2 h. The volume content, V_f, of the CFs is about 60 vol %. The thermal conductivity of CFRP is determined using Eq. (2) The thermal diffusivity is determined by the laser pulse heating method using a commercially available apparatus (Sinku-Riko, Inc., type TC-7000).[18,19] The specific heat capacity is determined using the DSC as was done for fibers. The thermal conductivity of CFRP can be estimated using the additive law

$$\lambda_{\mathrm{CFRP}}=V_f\lambda_{\mathrm{CF}}+(1-V_f)\lambda_{\mathrm{ER}}, \tag{32}$$

where λ_{ER} is the thermal conductivity of the epoxy resin, and is equal to 0.284 $\mathrm{W\,m^{-1}\,K^{-1}}$. Figure 12 shows the comparison between the directly observed thermal conductivity of CFRPs, λ_{obs}, and the thermal conductivity, λ_{est}, estimated using Eq. (32) from the values of CFs measured using the ac calorimetric method. The agreement between λ_{obs} and λ_{est} demonstrates the validity of the additive relation, Eq. (32) and the present results for CFs obtained by the ac calorimetric method.

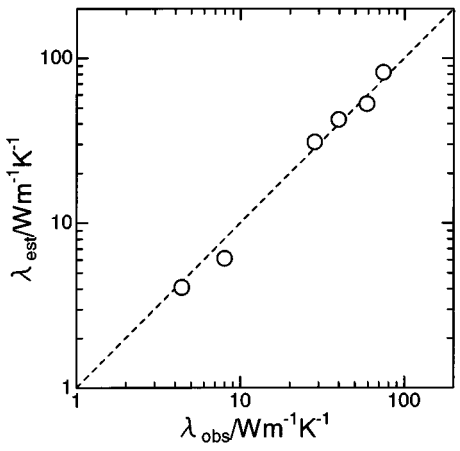

FIG. 12. The relation between observed thermal conductivity, λ_{obs}, and estimated thermal conductivity, λ_{est}, of unidirectional CFRP composites made of CFs at 298.15 K. The volume content of CFs is about 60 vol %. λ_{est} is estimated using the thermal conductivity of single-filament CFs obtained by the ac calorimetric method assuming the additivity relation, Eq. (32).

[1] R. Berman, *Thermal Conduction in Solids* (Clarendon, Oxford, 1976).
[2] J. Heremans and C. P. Beetz, Jr., Phys. Rev. B **32**, 32 (1981).
[3] L. Piraux, P. Coopmans, and J.-P. Issi, Measurement **5**, 2 (1987).
[4] J. H. Barkyoumb and D. J. Land, J. Appl. Phys. **78**, 905 (1995).
[5] I. Hatta, Y. Sasuga, R. Kato, and A. Maesono, Rev. Sci. Instrum. **56**, 1643 (1985).
[6] I. Hatta, H. Yao, R. Kato, and A. Maesono, Jpn. J. Appl. Phys. **29**, 2851 (1990).
[7] I. Hatta, R. Kato, and A. Maesono, Jpn. J. Appl. Phys. **26**, 475 (1987).
[8] Y. Gu and I. Hatta, Jpn. J. Appl. Phys. **30**, 1137 (1991).
[9] T. Yamane, S. Katayama, and M. Todoki, Rev. Sci. Instrum. **66**, 5305 (1995).
[10] H. S. Carslaw and J. C. Jaeger, *Conduction of Heat in Solids*, 2nd ed. (Oxford University Press, New York, 1959).
[11] Y. Gu, X. Tang, Y. Xu, and I. Hatta, Jpn. J. Appl. Phys. **32**, L1365 (1993).
[12] I. Hatta, R. Kato, and A. Maesono, Jpn. J. Appl. Phys. **25**, L493 (1986).
[13] Y. S. Touloukian, R. W. Powell, C. Y. Ho, and M. C. Nicolaou, *Thermophysical Properties of Matter, Thermal Diffusivity*, TPRC Data Services Vol. 10 (IFI/Plenum, New York, 1973).
[14] A. Sumida, K. Ono, and Y. Kawazu, Int. SAMPE Symp. Exhib. **34**, 2579 (1989).
[15] D. T. Grubb, K. Prasad, and W. Adams, Polymer **32**, 1167 (1991).
[16] Y. Gu and I. Hatta, Jpn. J. Appl. Phys. **30**, 1295 (1991).
[17] B. T. Kelly, *Physics of Graphite* (Applied Science, London, 1981).
[18] R. E. Taylor and K. D. Maglic, *Compendium of Thermophysical Property Measurement Methods*, Vol. 1, ''Survey of Measurement Techniques,'' edited by K. D. Maglic, A. Cezairliyan, and V. E. Peletsky (Plenum, New York, 1984).
[19] R. E. Taylor and K. D. Maglic, *Compendium of Thermophysical Property Measurement Methods*, Vol. 2, ''Recommended Measurement Techniques and Practices,'' edited by K. D. Maglic, A. Cezairliyan, and V. E. Peletsky (Plenum, New York, 1992).